Heliyon 9 (2023) e21850

Contents lists available at ScienceDirect

Heliyon

journal homepage: www.cell.com/heliyon

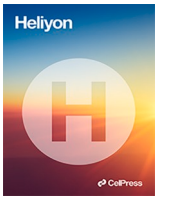

β-Cyclodextrin capped ZnS nanoparticles for CER-assisted colorimetric and spectrophotometric detection of Pb^{2+}, Cu^{2+}, and Hg^{2+} in an aqueous solution

Vyshnavi T. Veetil [a,b], Anakha D. Rajeeve [a,b], Saran G.P [a,b,1], K.S. Manish Kumar [a,b,1], M. Bhagiyalakshmi [c], Mari Vinoba [d], R. Yamuna [a,b,*]

[a] Department of Sciences, Amrita School of Physical Sciences Coimbatore, Amrita Vishwa Vidyapeetham, India
[b] Bio-materials Chemistry Research Laboratory, Amrita School of Engineering Coimbatore, Amrita Vishwa Vidyapeetham, India
[c] Department of Chemistry, Central University of Kerala, Periye, Kerala 671316, India
[d] Petroleum Research Center, Kuwait Institute for Scientific Research, Safat 13109, Kuwait

ARTICLE INFO

Keywords:
Heavy metal ions
β-Cyclodextrin
ZnS nanoparticles
Cation exchange reactions
Colorimetric sensor

ABSTRACT

Herein, simple, low-cost, and room-temperature synthesis of beta-cyclodextrin (β-CD) stabilized zinc sulfide nanoparticle (ZnS NP) through the chemical precipitation method has been reported for cation exchange reaction (CER) based colorimetric sensing of Pb^{2+}, Cu^{2+}, and Hg^{2+}. Formation of β-CD stabilized ZnS NPs (ZnS@β-CD) was verified by physicochemical characterization techniques such as XRD, XPS, FE-SEM, and TEM. ZnS@β-CD NPs showed color change selectively for the metal ions Pb^{2+}, Cu^{2+}, and Hg^{2+} among the various metal ions including Sn^{2+}, Cr^{3+}, Mn^{2+}, Fe^{3+}, Co^{2+}, Ni^{2+}, and Cd^{2+}. The solubility product of reactants and the transformed products are the reason for selective CER of ZnS@β-CD NPs towards Pb^{2+}, Cu^{2+}, and Hg^{2+} ions. ZnS@β-CD NPs dispersion revealed rapid color change from white to orange, black, and bright yellow on the addition of higher concentrations of Pb^{2+}, Cu^{2+}, and Hg^{2+} respectively. This color change is due to the formation of complete CER-transformed nanostructures such as PbS, CuS, and HgS in higher concentrations (10^{-1}- 10^{-3} M) of corresponding metal ions. The partial CER altered products $Zn_{1-x}Pb_xS$, $Zn_{1-x}Cu_xS$ and $Zn_{1-x}Hg_xS$ were detected due to the appearance of pale color in the lower metal ions concentrations of 10^{-4} - 10^{-6} M. This CER assisted transformation was also monitored through spectrophotometric methods. Moreover, infrared spectroscopic analysis was used to testify the structure of CER transformed product. The synthesized ZnS@β-CD NPs act as an efficient CER-based sensor for distinguishing and determining Pb^{2+}, Cu^{2+}, and Hg^{2+} at different level concentrations in the aqueous solution.

1. Introduction

Industrialization and urbanization caused the discharge of various types of contamination, such as heavy metal ions, pesticides, dyes, and pharmaceutical residues, into the aquatic system. Three main components in the atmosphere, specifically water, air, and soil, are incredibly polluted. Thus, for a sustainable environment, researchers are working continuously to design highly desirable materials

* Corresponding author. Department of Sciences, Amrita School of Physical Sciences Coimbatore, Amrita Vishwa Vidyapeetham, India.
E-mail address: r_yamuna@cb.amrita.edu (R. Yamuna).

[1] Saran G. P and K. S. Manish Kumar have contributed equally to this work.

https://doi.org/10.1016/j.heliyon.2023.e21850
Received 15 June 2023; Received in revised form 24 October 2023; Accepted 30 October 2023
Available online 4 November 2023
2405-8440/© 2023 Published by Elsevier Ltd. This is an open access article under the CC BY-NC-ND license (http://creativecommons.org/licenses/by-nc-nd/4.0/).

to explore a treatment technology in the interest of water decontamination [1,2]. The primary step in environmental protection is proper detection methods through qualitative and quantitative analyses. The subsequent step is the treatment of pollutants by different techniques. The presence of heavy metal ions in the water system is a severe issue due to their high toxicity and non-biodegradability [3]. Metals, including lead (Pb^{2+}), mercury (Hg^{2+}), and copper (Cu^{2+}), are among the most prevalent ones found in sewage. The sources of lead contamination in the environment are mainly from industrial, automotive exhaust emissions, melting and processing of ores. In contrast, other sources include lead batteries, additives of paints, and varnishes [4,5]. Pb^{2+} metal ion is one among the endocrine-disrupting chemicals (EDC) [6]. These EDC chemicals interfere with the hormonal system of the body. Long-term exposure to these chemicals can cause of lower IQ, delayed or impaired neurobehavioral development and other health ailments [7,8]. The copper metal ions discharged from industry and pesticides can cause diseases like Wilson's and vineyard sprayer's lung disease [9]. Mercury ion contamination is mainly from used thermometers, barometers, and tube lights. Microorganisms in the environment transform these discharged mercury ions into dangerous methylmercury compounds that can accumulate in the food chain and result in Minamata disease [10]. Thus, environmental monitoring of Pb^{2+}, Cu^{2+}, and Hg^{2+} ions in aqueous media becomes essential for minimizing such consequences on world health.

Recently, new nanomaterials, particularly chalcogenides, have been extensively synthesized using sequential cation exchange reactions (CER) at the nanoscale [11–13]. CER is advantageous due to its simplicity, tunable composition, and tunable color in colloidal nanostructure, and ability to maintain morphology. A literature study reveals that orange-colored CdSe transformed into a black-colored Ag_2Se gel due to the exchange of cations Cd^{2+} with Ag^{+}. During the process of CER, cations are comparatively mobile in the crystal lattice, whereas anions assist in retaining the structural framework [14]. Recent literature study supports CER's thermodynamic and kinetic favorability in nanometer-scale ionic crystals due to their large specific surface area and relative solubility between the reactant and the product [15]. Many studies have exploited CER-assisted fluorescent sensors to detect various metal ions [16–18]. Therefore, it would be ideal to have a sensor platform that derives CER-based naked-eye colorimetric responses for detecting heavy metal ions in aquatic environments.

A few studies have explored ZnS nanomaterials as a platform for CER-assisted colorimetric heavy metal detection [19]. For example, Amit Jaiswal *et al.* developed a chitosan film-impregnated ZnS quantum dots for the ion exchange-based colorimetric sensing and removal of Hg^{2+}, Ag^{+}, and Pb^{2+} ions in aqueous media [20]. In another work, Sumaiya Bano *et. al.* synthesized an aqueous starch-capped ZnS quantum dot as a CER-guided colorimetric sensor for the metal ions Pb^{2+}, Cu^{2+}, and Hg^{2+} in an aqueous solution [21]. Moreover, literature studies reveal that ZnS nanoparticles (NPs) synthesis focus mainly on the non-aqueous media at high temperature and pressure [22,23]. Nevertheless, sensing research is often performed in an aqueous medium or a mixture of water/organic solvents. Consequently, there is a practical constraint in using non-aqueous ZnS NPs in environmental domains. Consequently, developing an easy and cost-effective method for synthesizing ZnS NPs in an aqueous medium is essential, preferably at room temperature.

Cyclodextrins are macrocyclic supramolecular capping agents that can alter the shape and physicochemical characteristics of the NPs [24,25]. Using a capping agent during nanoparticle synthesis can reduce aggregation through steric hindrance and surface passivation. Moreover, it can help in improving the biocompatibility and hydrophilicity of NPs [26]. Literature studies reveal that β-CD functionalized gold NPs were utilized for the colorimetric detection of Pb^{2+}, and Cu^{2+} metal ions [27,28]. Furthermore, β-CD capped gold-iron NP has been reported for the colorimetric detection of Cr^{2+} metal ions [29]. However, none of the studies have used β-CD capped NPs for CER-assisted heavy metal detection. The synthesis of ZnS NPs using β-CD as the capping agent has not been reported so far in the literature.

Here, we report the simple, low-cost, and room-temperature synthesis of β-CD stabilized ZnS (ZnS@β-CD) NPs through the chemical precipitation method. Synthesized ZnS NPs are used as a CER-guided colorimetric sensor for metal ions such as Pb^{2+}, Cu^{2+}, and Hg^{2+}. ZnS@β-CD NPs dispersion showed a rapid color change from white to orange, black, and bright yellow after adding 10^{-1} - 10^{-3} M concentrations of Pb^{2+}, Cu^{2+}, and Hg^{2+} metal ions, respectively. This color change is due to converting ZnS NPs to PbS, CuS, and HgS nanostructures (NSs) after the entire CER at higher concentrations of respective metal ions. On the contrary, it is converted to $Zn_{1-x}Pb_xS$, $Zn_{1-x}Cu_xS$ and $Zn_{1-x}Hg_xS$ by partial CER at lower concentrations of respective metal ions. The color of the ZnS NP solution is tunable according to the concentration of respective metal ions. This color change indicates that the ZnS@β-CD NPs efficiently distinguish and determine the different concentrations of these metal ions. UV–Visible photometric analysis further confirmed the colorimetric reactions of ZnS@β-CD NPs towards the above metal ions. This proposed work offers a promising colorimetric sensing platform for heavy metal ion detection in water bodies.

2. Materials and methods

2.1. Materials

Zinc nitrate hexahydrate ($[Zn(NO_3)_2{\cdot}6H_2O]$; Avra chemicals), sodium sulfide flakes (Na_2S; Sisco Research Laboratories), and β-cyclodextrin (β-CD; Moly Chem) were used as received, and all these chemicals were of an analytical grade. Double distilled water (DDW) was used as a solvent for the experiments.

2.2. Synthesis of ZnS@β-CD

ZnS@β-CD NPs were prepared using the chemical precipitation method at room temperature. In a typical experimental procedure, $Zn(NO_3)_2{\cdot}6H_2O$ (0.341 g, 0.002 mol) and β-CD (1.021 g, 0.001 mol) were mixed with 30 mL DDW in the round bottom flask. This

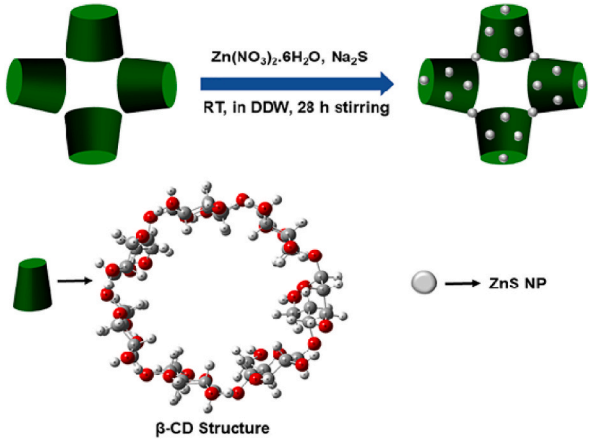

Scheme 1. Schematic diagram for the synthesis of ZnS@β-CD NPs.

mixture was entirely dissolved by sonicating for a few minutes and then stirred for 1 h on the magnetic stirrer. Then, Na_2S (0.09 mol) was dissolved in 50 mL DDW and added dropwise into the reaction mixture. A White precipitate was formed during the addition of Na_2S. Further, the reaction mixture was stirred for 28 h. After completion of the chemical reaction, ZnS@β-CD NPs were acquired by centrifugation at 6000 rpm for 10 min. The obtained residue was washed five times with DDW to remove the excess Na_2S and dried at 80 °C for 24 h in a hot air oven.

2.3. Selectivity studies of ZnS@β-CD NPs towards various heavy metal ions

A colloidal solution of ZnS NP was prepared by dispersing 50 mg of ZnS@β-CD NP in 100 mL DDW by sonicating the reaction mixture for 15 min. Then, it was centrifuged for 5 min at 3000 rpm to get the fine colloidal dispersion. 5 mL of this colloidal solution was taken in different glass vials. 0.5 mL of 10^{-3} M solution of various metal ions (Sn^{2+}, Pb^{2+}, Cr^{3+}, Mn^{2+}, Fe^{3+}, Co^{2+}, Ni^{2+}, Cu^{2+}, Cd^{2+} and Hg^{2+}) were added to each of these glass vials. UV–Visible absorption spectra of each solution were recorded after shaking the solution well for 5 min and photographed.

2.4. Cation exchange reactions of ZnS@β-CD NPs with Pb^{2+}, Cu^{2+}, and Hg^{2+} metal ions

Six different concentrations (10^{-6}, 10^{-5}, 10^{-4}, 10^{-3}, 10^{-2}, and 10^{-1} M) of metal ions Pb^{2+}, Cu^{2+}, and Hg^{2+} were made and used for the CER reactions with ZnS@β-CD NPs. 0.5 mL of these metal ion solution was added to 5 mL of ZnS NPs colloidal solution taken in different glass vials. UV–Visible absorption spectra of each solution were recorded after shaking the solution well for 5 min and photographed. Further, we monitored time-resolved metal-ZnS interactions by colorimetrically as well as spectrophotometrically.

2.5. Characterization

The purity, relative phase, and structure of the ZnS@β-CD NPs were analyzed through X-ray diffraction techniques (XRD) (model: Malvern Panalytical multipurpose) with radiation source (Cu Kα; $\lambda = 0.154$ nm, 40 kV, 30 mA). Optical absorbance and metal ion sensing behavior of ZnS@β-CD NPs were studied using UV–Visible spectrophotometer (model: Shimadzu UV – 1800) in the spectral range 200–800 nm. Scanning electron microscopy (SEM-EDX) (Carl Zeiss, German; model – ZEISS Gemini SEM 300) was used to analyze sample surface morphology and elemental analysis. Transmission Electron Microscope (HR-TEM) (model: TECHNAI-FEI, The Netherlands) was used to find ZnS@β-CD NPs structure and particle size. X-Ray photoelectron spectra (XPS) of ZnS@β-CD NPs were recorded using Kratos Axis Ultra, UK with monochromatic 96 W power Al Kα radiation. Studied the chemical structure of ZnS@β-CD NPs and its CER transformed products using Fourier-Transform Infrared (FT-IR) spectra (model: Bruker (Alpha Platinum) in ATR mode.

3. Results and discussion

3.1. Synthesis and characterization of ZnS@β-CD NPs

ZnS@β-CD NPs were prepared using the chemical precipitation method at room temperature. We optimized the synthesis of ZnS@β-CD NPs after carrying out several trials with the different mole ratio of precursor ($Zn(NO_3)_2{\cdot}6H_2O$), capping agent (β-CD), and Na_2S. Initially, the reactions were carried out using 1:1, 1:2, and 2:1 mol ratio of precursor and capping agent. Further, the obtained product purity was analyzed by using FT-IR spectroscopy. Analysis of FT-IR spectrum reveals that 2:1 (precursor: capping agent) mole ratio shown the peaks correspond to pure ZnS NPs as compared to 1:1 and 1:2 mol ratio of precursor and capping agent. Further, the

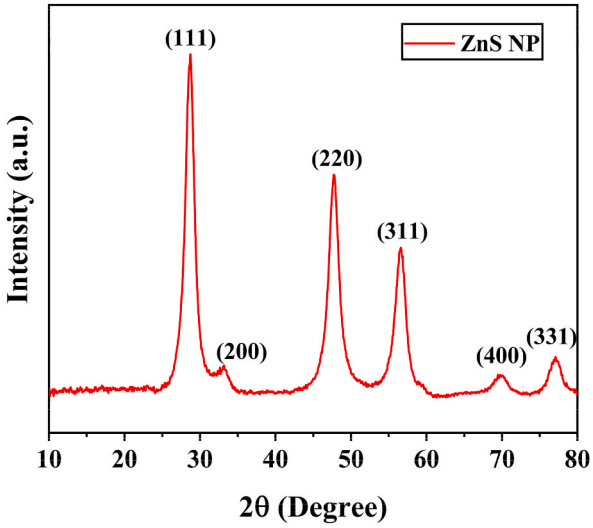

Fig. 1. XRD patterns of ZnS@β-CD NPs.

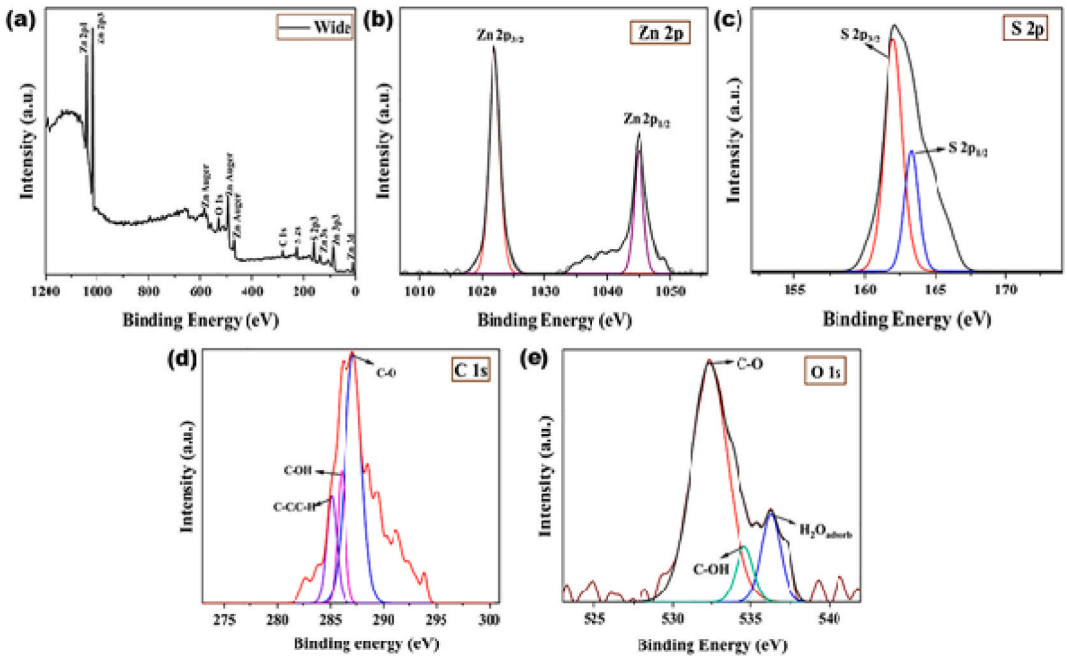

Fig. 2. The XPS analysis of ZnS@β-CD NPs (a) Wide scan XPS (b) Zn 2p deconvoluted peaks (c) S 2p deconvoluted peaks (d) C 1s deconvoluted peaks, (e) O 1s deconvoluted peaks.

yield of the reaction was optimized based on the concentration and dilution of Na_2S. Thus, we obtained better yield and pure ZnS NPs when we used 0.09 M of Na_2S in 50 mL of DDW. The scheme for the synthesis of ZnS@β-CD NPs is shown in Scheme 1.

Structural identification of ZnS@β-CD NPs has been done with XRD pattern as shown in Fig. 1. The XRD pattern indicated $2\boldsymbol{\theta}$ peaks at 28.72°, 33.16°, 47.83°, 56.5°, 69.90°, and 77.08° that are attributed to the lattice planes (111), (200), (220), (311), (400) and (331), respectively. These peaks align with those of JCPDS data card number 05–0566 and confirm face-centered cubic phase of ZnS [30]. All these peaks intensity does not deviate from the JCPDS-05-0566 file intensities. The mean crystallite size of ZnS@β-CD NP was found out from Debye-Scherrer formula $D = k\lambda/\boldsymbol{\beta}\cos\boldsymbol{\theta}$, where D indicates crystallite size, k is Scherrer's constant, which is 0.94, $\boldsymbol{\lambda}$ is the wavelength of X-rays (Cu Kα radiation, $\lambda = 0.1540$ nm), $\boldsymbol{\theta}$ is the Bragg's diffraction angle, and $\boldsymbol{\beta}$ is the full width at half-maximum (FWHM) of that peak in radian [31]. The mean crystallite size of ZnS@β-CD NPs were found to be 19.78 nm.

The elemental composition and purity of ZnS@β-CD NPs were investigated using XPS techniques. Fig. 2 (a)-(e) shows the obtained XPS spectra. The wide XPS spectra in Fig. 2 (a) indicate the peaks corresponding to C, O, Zn Auger, satellite peaks of Zn and S. C and O

Table 1
Elemental analysis based on XPS data for ZnS@β-CD NPs.

Peak	Position (Binding energy (eV))	Atomic%
C 1s	285.15	23.97
O 1s	532.35	14.79
Zn 2p	1021.95	33.07
S 2p	162.05	28.17

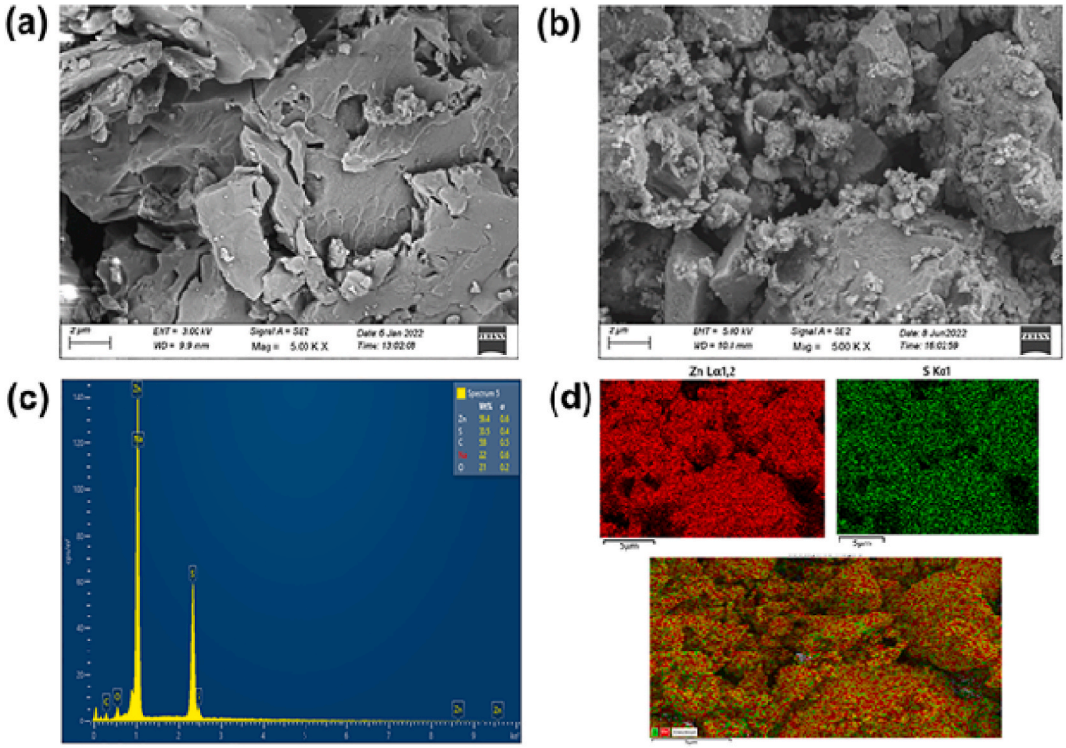

Fig. 3. (a) SEM Image of β-CD, (b) SEM image of ZnS@β-CD NPs, (c) EDX spectra of ZnS@β-CD NPs, (d) Elemental mapping images of ZnS@β-CD NPs.

XPS peaks confirm the presence of capping agent (β-CD). Table 1 depicts the atomic weight percentage of elements in the ZnS@β-CD NPs. It is evident that the sample contains a higher fraction of Zn atoms than S atoms which implies a non-stoichiometric composition and the development of sulfur vacancies in the structure [32]. The deconvoluted core level spectrum of Zn 2p is shown in Fig. 2 (b). The spectra reveal binding energy peaks at 1021.95 eV (Zn $2p_{3/2}$) as well as 1045.05 eV (Zn $2p_{1/2}$) with a characteristic peak difference of 23.1 eV [33], which confirms the presence of Zn^{2+} ions in the sample. The deconvoluted XPS spectra of S 2p in Fig. 2 (c) have been divided into two distinctive peaks at 162.05 eV (S $2p_{3/2}$) and 163.35 eV (S $2p_{1/2}$) with an energy splitting of 1.3 eV [34]. These peaks are attributed to S^{2-} ions in the ZnS NPs. The C 1s deconvoluted spectra in Fig. 2 (d) give binding energy peaks at 285.15, 286.05, and 287.25 eV corresponding to *C*–C/C–H, *C*–OH, and *C*–O, respectively [35,36]. The O 1s deconvoluted spectra in Fig. 2 (e) show peaks at 532.35, 534.55, and 536.25 eV of binding energies, and these correspond to *C*–O, *C*–OH and surface adsorbed H_2O, respectively [37, 38]. These C 1s and O 1s spectra endorse the β-CD capping agent in the ZnS NP sample.

3.2. *Morphology studies of ZnS@β-CD NPs*

The morphology of ZnS@β-CD NPs was examined by performing the FE-SEM analysis. In Fig. 3 (a), irregular flake-like morphology is attributed to β-CD [39]. However, the SEM image of ZnS@β-CD NPs in Fig. 3 (b) illustrates spherical-shaped NPs were incorporated on the surface of flake shaped β-CD. The SEM-EDX analysis confirmed further purity of the ZnS@β-CD NPs. The EDX spectra in Fig. 3 (c) document the presence of Zn, S, C, and O with a weight % of 59.4, 30.5, 5.8, and 2.1, respectively. Moreover, the elemental mapping images in Fig. 3 (d) reveal the spatial distribution of Zn and S elements within the sample.

TEM analysis was performed to find out the shape and size of synthesized ZnS@β-CD NPs. Fig. 4 (a)-(d) depict the TEM micrographs of ZnS@β-CD NPs, histogram, and the SAED pattern. TEM images clearly illustrate that the ZnS NPs are spherical in shape. The particle

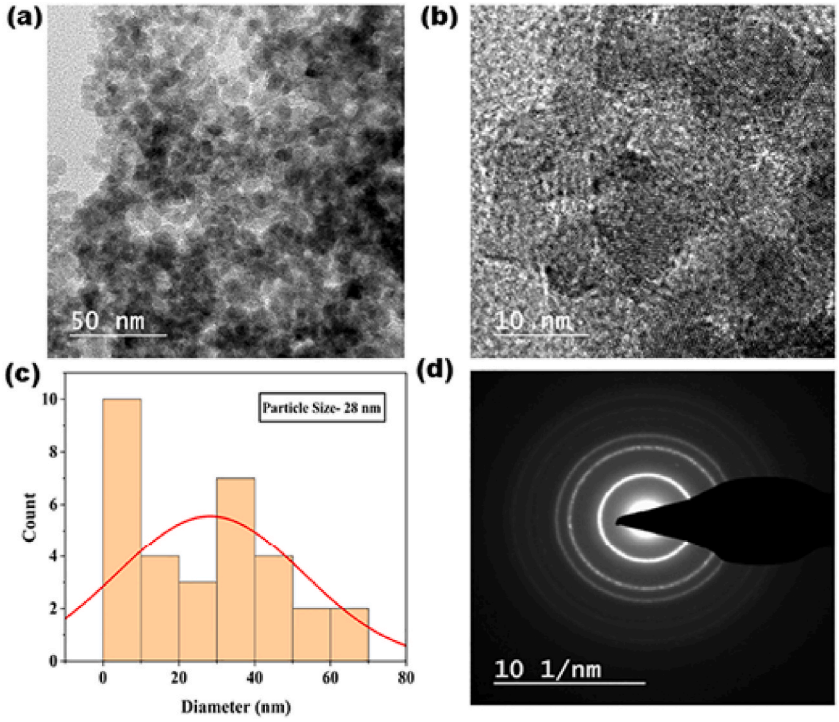

Fig. 4. HR-TEM images of ZnS@β-CD NPs at various scale (a) 50 nm, (b) 10 nm, (c) Particle size distribution histogram, (d) SAED pattern.

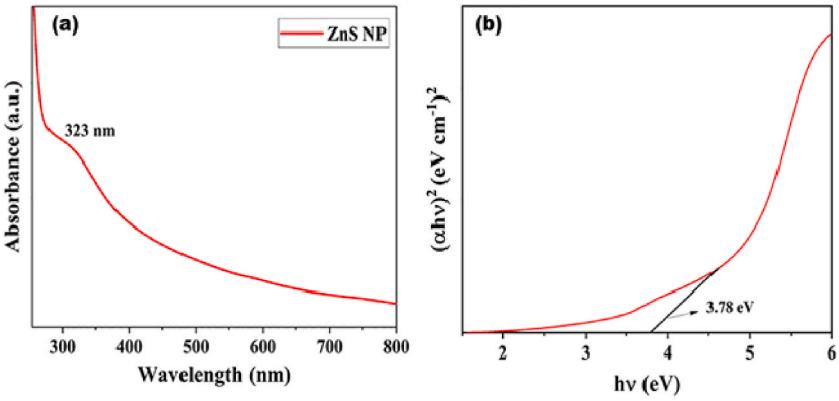

Fig. 5. (a) UV–Visible absorption spectrum and (b) Tauc plot of ZnS@β-CD NPs.

size distribution of ZnS@β-CD NPs was determined by plotting the histogram curve with the help of ImageJ software. The size distribution graph depicts the mean diameter of the ZnS@β-CD NPs is 28 nm, more significant than that obtained by XRD. The observation is because XRD provides only the sample's crystallite size, whereas TEM image provides entire particle size, including non-crystalline components [40]. Fig. 4 (d) shows the selected area electron diffraction (SAED) pattern of ZnS@β-CD NPs. The diffraction pattern comprises a center hole surrounded by wide concentric rings. The rings correspond to reflections from the planes (1 1 1), (2 2 0), and (3 1 1) which confirm the cubic structure of ZnS NPs [41]. The distinct bright spots in the SAED image ensure the polycrystalline nature of the synthesized ZnS@β-CD NPs [42].

3.3. Optical properties of ZnS@β-CD NPs

Fig. 5 represents the UV–Visible and Tauc plot of ZnS@β-CD NPs. Fig. 5a depicts a peak at 323 nm in the UV region, which is assigned to the band gap absorption of ZnS [39]. The optical band gap (Eg) can be determined with Tauc plot by extrapolating the linear region of $(\alpha h\upsilon)^2$ vs hυ plots and from the intercept of hυ axis as shown in Fig. 5b. The condition is depicted as; $(\alpha h\upsilon)^{1/n} = C \times (h\upsilon - Eg)$, where α denotes absorption coefficient, h refers to Planck's constant, C represents the proportionality constant, ν is the light

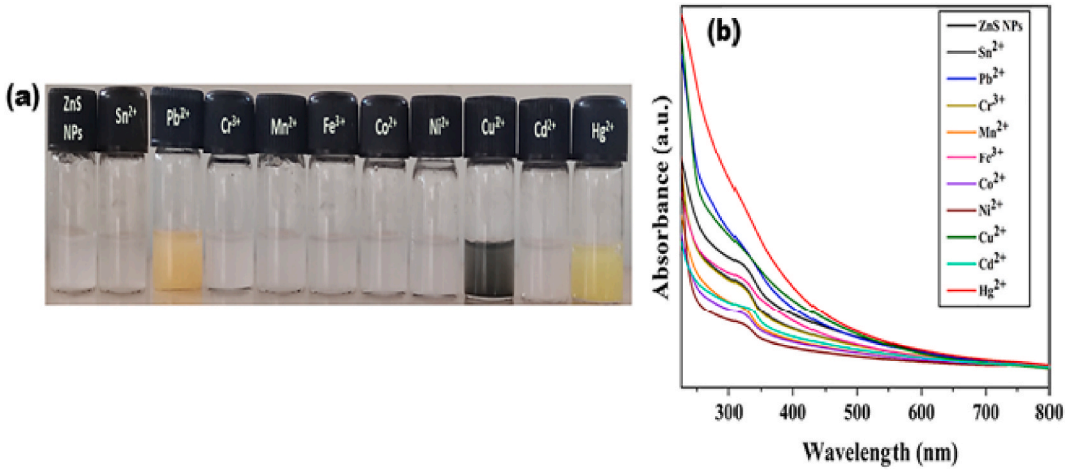

Fig. 6. (a) Colorimetric and (b) UV–Visible spectroscopic analysis of ZnS@β-CD NPs towards different metal ions.

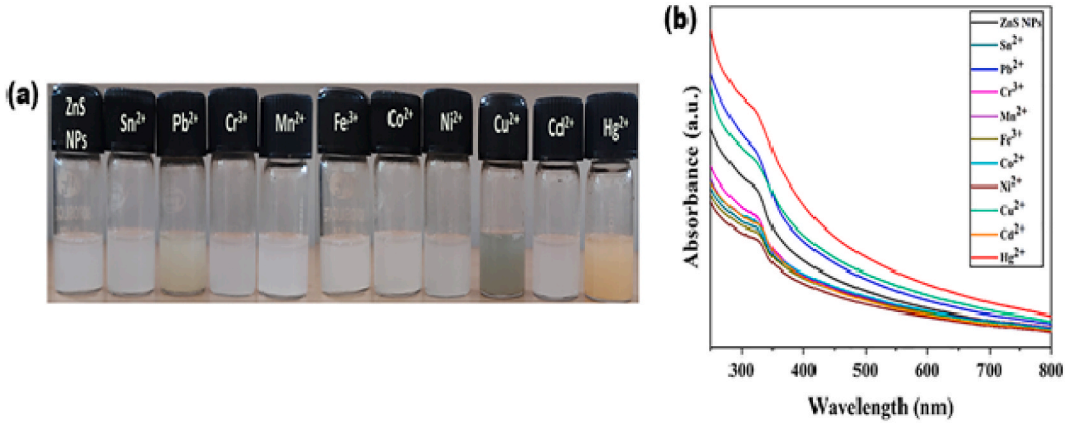

Fig. 7. (a) Colorimetric and (b) UV–Visible spectroscopic analysis of ZnS NPs (without β-CD) towards different metal ions.

frequency, Eg indicates bandgap, and n is 1/2 for direct bandgap material [43]. The band gap energy of the ZnS@β-CD NPs is found to be 3.78 eV. In contrast, the absorbance of bulk ZnS is reported to be 340 nm with a band gap energy of 3.6 eV [44]. This blue shift indicates the formation of ZnS@β-CD NPs.

3.4. Selectivity studies of ZnS@β-CD NPs towards various heavy metal ions

The selectivity of ZnS@β-CD NPs was studied using 10^{-3} M solution of various metal ions such as Sn^{2+}, Pb^{2+}, Cr^{3+}, Mn^{2+}, Fe^{3+}, Co^{2+}, Ni^{2+}, Cu^{2+}, Cd^{2+} and Hg^{2+}. The colorimetric analysis of ZnS@β-CD NPs was determined using fine colloidal dispersion of ZnS@β-CD NPs in DDW, which was achieved by sonicating ZnS@β-CD NPs in DDW for 10 min and followed by centrifugation. Furthermore, 5 mL of colloidal dispersion was taken in a series of labeled glass vials. A 0.5 mL of various metal ions solution were added to each vial. Photographed their colorimetric responses after 5 min, as shown in Fig. 6 (a). The white-colored ZnS colloidal dispersion was changed to orange, black, and bright yellow after adding metal ions Pb^{2+}, Cu^{2+}, and Hg^{2+}, respectively. Only these three metal ions showed a colorimetric response. ZnS colloidal dispersion showed no color change for other metal ions. Further, the selectivity of ZnS NPs was confirmed by performing UV–Visible photometric analysis. Fig. 6 (b) depicts the UV–Visible absorption spectra of ZnS@β-CD NPs in the presence of different metal ions, which indicates the disappearance of ZnS NP absorption band at 323 nm on the addition of Pb^{2+}, Cu^{2+}, and Hg^{2+} metal ions. At the same time, no significant change is observed for other metal ions. This result further confirms the selectivity of ZnS@β-CD NPs towards Pb^{2+}, Cu^{2+}, and Hg^{2+}. The selectivity of ZnS@β-CD NPs for CER-based metal detection is largely attributed to the solubility product (Ksp) of the reactant and product. Higher Ksp value of ZnS readily undergoes CER with Pb^{2+}, Cu^{2+}, and Hg^{2+} ions and forms lower Ksp value of PbS, CuS, and HgS. However, other heavy metal sulfide formation is difficult due to their higher Ksp value [21].

Further, the influence of β-CD capping agent on the CER metal sensing ability of ZnS NP was evaluated by comparing the selectivity of unmodified ZnS NP and ZnS@β-CD NP towards various heavy metal ions. Unmodified ZnS NPs were synthesized by following the

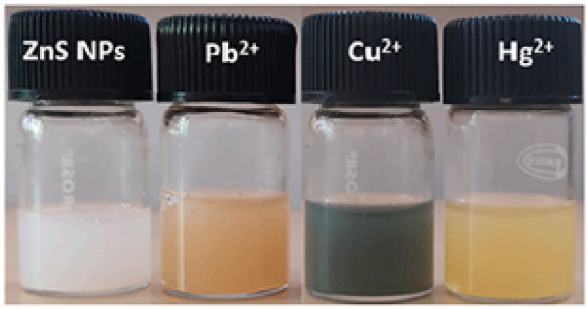

Fig. 8. Colorimetric responses of ZnS@β-CD NPs towards Pb^{2+}, Cu^{2+}, and Hg^{2+} in presence of other heavy metal ions.

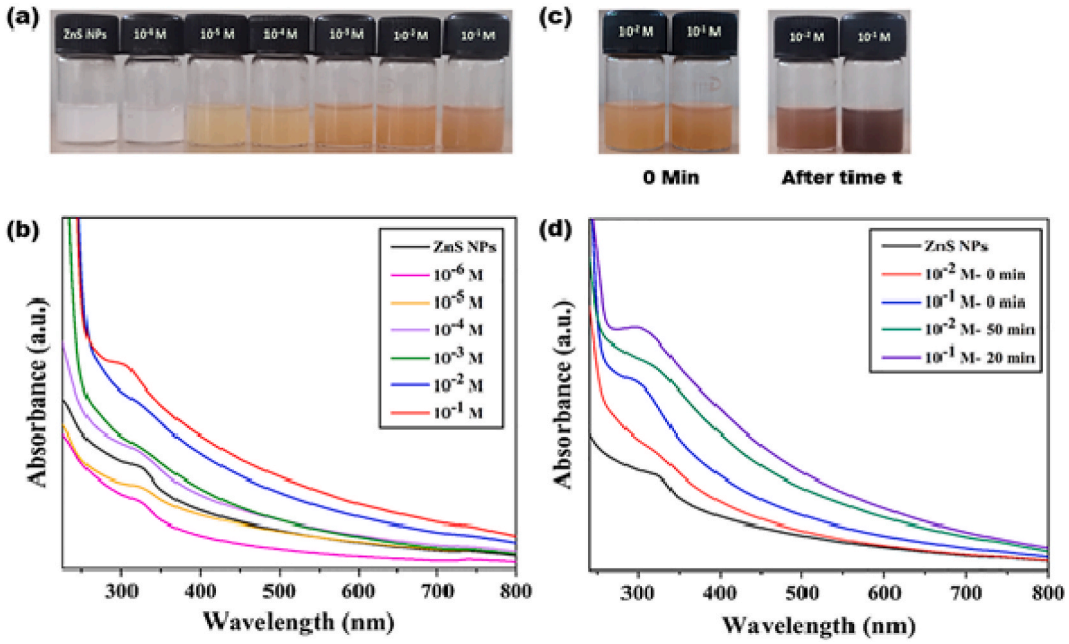

Fig. 9. (a) Colorimetric and (b) UV–Visible spectroscopic analysis of ZnS@β-CD NPs towards different concentrations of Pb^{2+}. Time-resolved interactions of ZnS@β-CD NPs with Pb^{2+}: (c) Photographs of 10^{-2} M and 10^{-1} M of Pb^{2+} at 0 min and after time t (50 min for 10^{-2} M and 20 min for 10^{-1} M). (d) Time-based UV–Visible spectroscopic analysis of 10^{-2} M and 10^{-1} M of Pb^{2+} metal ions.

same procedure used for ZnS@β-CD NPs except the addition of capping agent β-CD. Then selectivity of unmodified ZnS NPs was studied using 10^{-3} M solution of various metal ions such as Sn^{2+}, Pb^{2+}, Cr^{3+}, Mn^{2+}, Fe^{3+}, Co^{2+}, Ni^{2+}, Cu^{2+}, Cd^{2+}, and Hg^{2+}. 5 mL of unmodified ZnS NPs colloidal dispersion in DDW was taken in a series of glass vials. 0.5 mL of various metal ions solution was added into each vial. After 5 min, colorimetric reactions were photographed, as shown in Fig. 7 (a). The ZnS colloidal dispersion slowly changes its color to a very pale black or pale yellow color after the addition of Cu^{2+} and Hg^{2+} metal ions, respectively. However, the addition of Pb^{2+} metal ions into ZnS colloidal dispersion reveal that the color change is very negligible. On the other hand, CER colorimetric response of ZnS@β-CD NPs was immediate and gave intense color change in the presence of Pb^{2+}, Cu^{2+}, and Hg^{2+} metal ions. Therefore, this comparative study proves the superior CER colorimetric response of ZnS@β-CD NPs towards Pb^{2+}, Cu^{2+}, and Hg^{2+} metal ions over unmodified ZnS NPs.

The selectivity of unmodified ZnS NPs was also confirmed by UV–Visible photometric analysis. Fig. 7 (b) illustrates the UV–Visible absorption spectra of unmodified ZnS NP and after the addition of different metal ions. The spectrum shows that unmodified ZnS NP gives an absorption band at 328 nm, which is red-shifted from 323 nm of ZnS@β-CD NPs. This indicates a slight increase in the size of uncapped ZnS NP compared to the size of ZnS@β-CD NPs. The spectrum also depicts that the addition of 10^{-3} M solution of Pb^{2+}, Cu^{2+}, and Hg^{2+} ions resulted in only a slight decrease in the absorption peak of ZnS NPs. This implies that complete CER transformation does not happen with the unmodified ZnS NPs. Meanwhile, no change is observed in the absorption peak of ZnS NPs with the addition of other metal ions as in the case of ZnS@β-CD. However, ZnS@β-CD NPs added with 10^{-3} M solution of Pb^{2+}, Cu^{2+}, and Hg^{2+} ions showed the complete disappearance of ZnS absorption peak as shown in Fig. 6. As a result, ZnS@β-CD NPs have higher CER spectrophotometric response towards Pb^{2+}, Cu^{2+}, and Hg^{2+} ions than uncapped ZnS NPs. Therefore, β-CD capping agent not only reduces the size of ZnS NPs

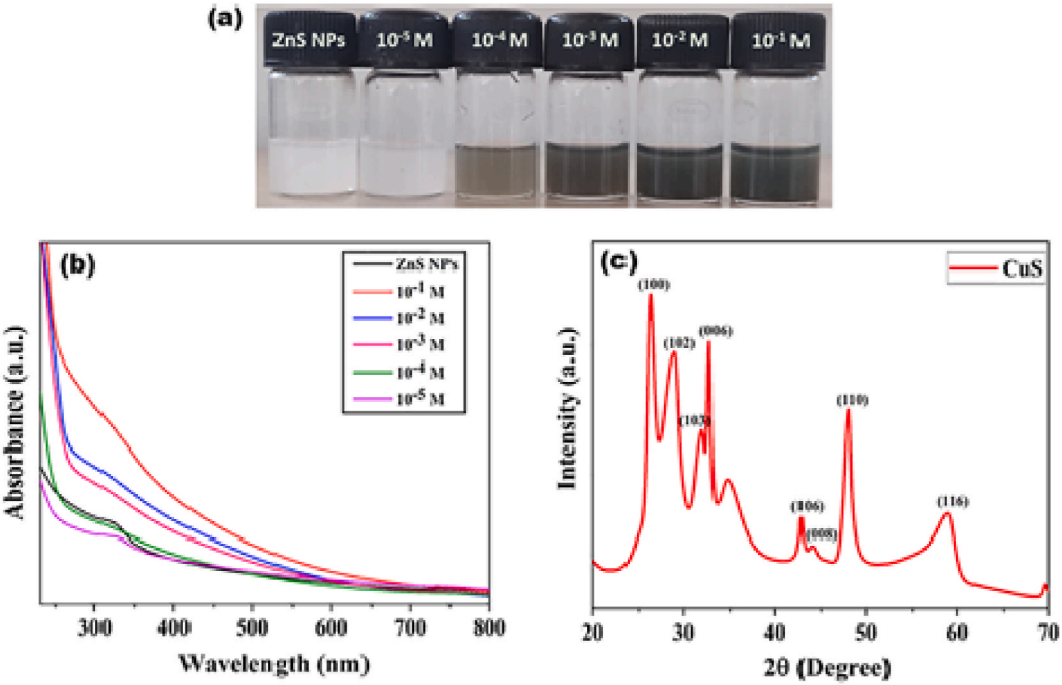

Fig. 10. (a) Colorimetric and (b) UV–Visible spectroscopic measurements of ZnS@β-CD NPs towards different concentrations of Cu^{2+}, (c) XRD pattern of CuS NS.

and enhances the CER sensing capabilities.

3.5. Interference studies

The interference of other metal ions such as Sn^{2+}, Cr^{3+}, Mn^{2+}, Fe^{3+}, Co^{2+}, Ni^{2+}, and Cd^{2+}on the sensing ability of ZnS@β-CD NPs towards Pb^{2+}, Cu^{2+}, and Hg^{2+} ions was analyzed. Typically, 5 mL of ZnS@β-CD NPs colloidal solution taken in 3 different glass vials were added with 3 drops of 10^{-3} M solution of Sn^{2+}, Cr^{3+}, Mn^{2+}, Fe^{3+}, Co^{2+}, Ni^{2+}, and Cd^{2+} ions. Then, their colorimetric response was checked by adding 3 drops of respective 10^{-3} M solution of Pb^{2+}, Cu^{2+}, and Hg^{2+} ions. The color change observed after 5 min was provided in Fig. 8, wherein, white-colored ZnS NP colloidal solution changed to orange, black, and bright yellow after adding metal ions Pb^{2+}, Cu^{2+}, and Hg^{2+}, respectively. Thus, it can be verified that other metal ions in the ZnS NP colloidal solution do not interfere with its colorimetric response towards Pb^{2+}, Cu^{2+}, and Hg^{2+} ions.

3.6. Cation exchange reactions of ZnS@β-CD NPs with Pb^{2+}

Colorimetric analysis of ZnS@β-CD NPs were recorded in the presence of different concentrations of (10^{-6}, 10^{-5}, 10^{-4}, 10^{-3}, 10^{-2}, and 10^{-1} M) Pb^{2+} solution. 0.5 mL of Pb^{2+} solution was added to 5 mL of ZnS colloidal solution, and their colorimetric response was photographed after 5 min. The photograph (Fig. 9 (a)) indicates that white colored ZnS colloidal solution showed the color change in the presence of different Pb^{2+} concentrations. ZnS NPs solution turned to pale yellow color for lower Pb^{2+} ions concentration (10^{-4} - 10^{-6} M). In contrast, it turned orange for higher Pb^{2+} ions concentration (10^{-1} - 10^{-3} M), indicating that the ZnS@β-CD NP is efficiently distinguishes and determines the different Pb^{2+} ions concentrations.

Furthermore, the UV–Visible spectroscopic analysis of ZnS@β-CD NPs in the presence of different Pb^{2+} ions concentrations were studied, as shown in Fig. 9 (b). The spectrum indicates that at 10^{-4} - 10^{-6} M of Pb^{2+}, the absorption band of ZnS NP was decreased, and the solution's color changed to pale yellow, which may be owing to the interaction of Pb^{2+} and S^{2-}. The absorption peaks of ZnS NPs disappeared entirely, and the solution color turned to pale orange at a concentration of 10^{-3} - 10^{-2} M. A partial cation exchange process began between Pb^{2+} ion and Zn^{2+} ion, resulting in the production of $Zn_{1-x}Pb_xS$ NSs. The value of x increases with increase in the concentration of Pb^{2+} ion. Cation exchange reaction increases at 10^{-1} M of Pb^{2+} ion concentration leading to a new absorption peak at 303 nm, accompanied by a colorimetric shift from white to orange.

In addition, time-dependent colorimetric and spectroscopic investigations were carried out on ZnS NPs using 10^{-6} – 10^{-1} M Pb^{2+} metal ion solution, as shown in Fig. 9 (c) and (d). Even after 2 h, there was no discernible change in the color and absorption spectra of the 10^{-6} –10^{-3} M solutions. However, after 50 and 20 min of exposure, the orange-colored 10^{-2} and 10^{-1} M Pb^{2+} solutions became brown. Therefore, UV–Visible absorption responses were recorded before (0 min) and after the color change. When comparing to 0 min absorbance, the spectra reveal that their absorbance increases significantly after the color change. The shift in UV–vis absorption peak

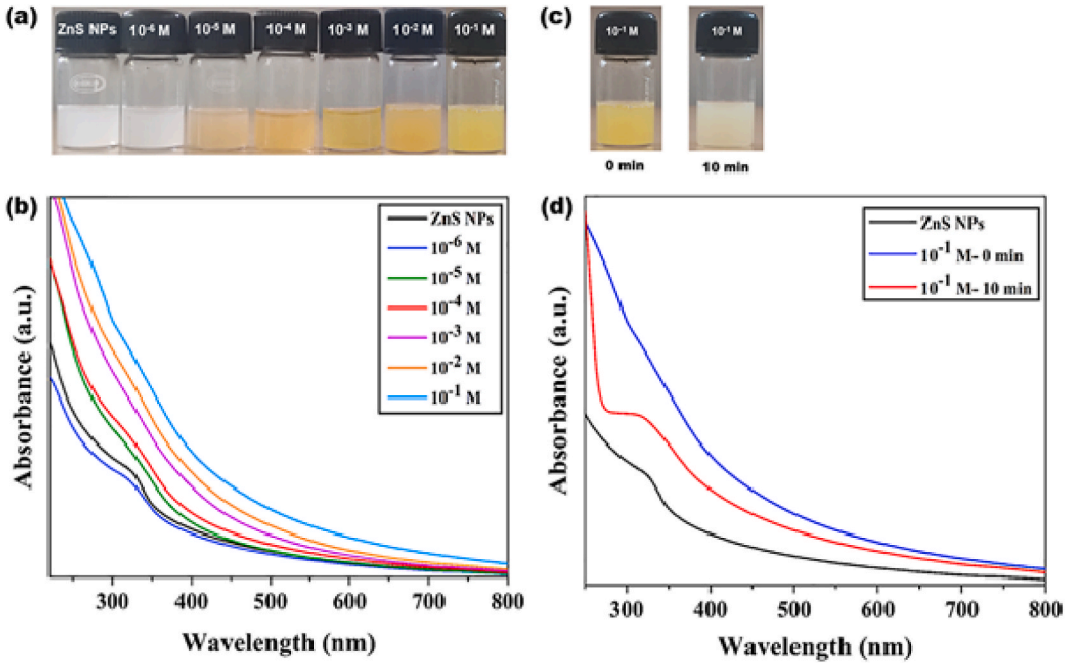

Fig. 11. (a) Colorimetric and (b) UV–Visible spectroscopic measurements of ZnS@β-CD NPs towards different concentrations of Hg^{2+}. Time-resolved interactions of ZnS@β-CD NPs with Hg^{2+}: (c) Photograph of 10^{-1} M of Hg^{2+} at 0 min and after 10 min. (d) Time-based UV–Visible spectroscopic responses of 10^{-1} M of Hg^{2+}.

at 303 nm reveals nearly complete cation exchange processes and implies the development of PbS NSs. These findings demonstrate that the color, composition, and wavelength can be tuned via CER of Pb^{2+} with ZnS@β-CD NPs.

3.7. Cation exchange reactions of ZnS@β-CD NPs with Cu^{2+} ions

ZnS@β-CD NPs colorimetric analysis was studied in the presence of Cu^{2+} solution at concentrations ranging from 10^{-5}, 10^{-4}, 10^{-3}, 10^{-2}, and 10^{-1} M. For this, 0.5 mL of Cu^{2+} solution was added to 5 mL of ZnS colloidal solution, and the colorimetric reaction was captured after 5 min. The photograph (Fig. 10 (a)) shows that white colored ZnS colloidal solution exhibited a color change in the presence of different concentrations of Cu^{2+} solutions. For lower concentrations of Cu^{2+} solutions, ZnS solution turned pale black color, whereas, for higher concentrated Cu^{2+}, it instantly turned black, which reveals that the ZnS@β-CD NPs effectively identify and measure the various Cu^{2+} ion concentrations.

The UV–Visible spectroscopic measurements of ZnS@β-CD NPs in various Cu^{2+} ion concentrations were also investigated. The spectrum in Fig. 10 (b) showed that the absorption peak associated with ZnS NP reduced, and the solution color changed to pale black at 10^{-5} - 10^{-4} M of Cu^{2+}, which may be due to the interaction of Cu^{2+} with S^{2-}. The solution color change indicates the production of $Zn_{1-x}Cu_xS$ NSs due to the partial CER reaction. In contrast, higher Cu^{2+} concentrations (10^{-3} –10^{-1} M) resulted in the complete disappearance of ZnS NP's absorbance peak and a prominent rise in absorbance. Later, time-resolved studies were carried out for all the Cu^{2+} concentrations by recording their colorimetric and UV–Visible spectroscopic responses. However, no discernible change was observed even after 2 h of exposure. This observation reveals the immediate occurrence of nearly complete cation exchange processes and implies the development of CuS NSs. Further, the formation of CuS NS was confirmed using XRD measurement, as shown in Fig. 10 (c). The XRD patterns clearly show peaks at (100), (102), (103) (006), (106), (008), (110), and (116) planes that correspond to the standard data for the hexagonal phase of the CuS covellite structure (JCPDS No.06-0464). The mean crystallite size of CuS was calculated to be 3.52 nm from Debye-Scherrer equation.

3.8. Cation exchange reactions of ZnS@β-CD NPs with Hg^{2+} ions

ZnS@β-CD NPs colorimetric responses were investigated in the presence of Hg^{2+} solution at the concentrations ranging from 10^{-6}, 10^{-5}, 10^{-4}, 10^{-3}, 10^{-2}, and 10^{-1} M. For this, 0.5 mL of Hg^{2+} solution was added to 5 mL of ZnS colloidal solution, and the colorimetric reaction was recorded after 5 min. The photograph (Fig. 11 (a)) shows that white colored ZnS colloidal solution displayed a color change in the presence of different concentrations of Hg^{2+} solutions. On exposure to lower concentrations of Hg^{2+} solutions, the color of ZnS solution turned to a pale yellow. In contrast, for higher concentrated Hg^{2+} it instantaneously turned to bright yellow color, which confirms that the ZnS@β-CD NPs are effective in identifying and quantifying the different Hg^{2+} ion concentrations.

Fig. 11 (b) depicts the UV–Visible spectroscopic analysis of ZnS@β-CD NPs in various Hg^{2+} ion concentrations. The spectrum

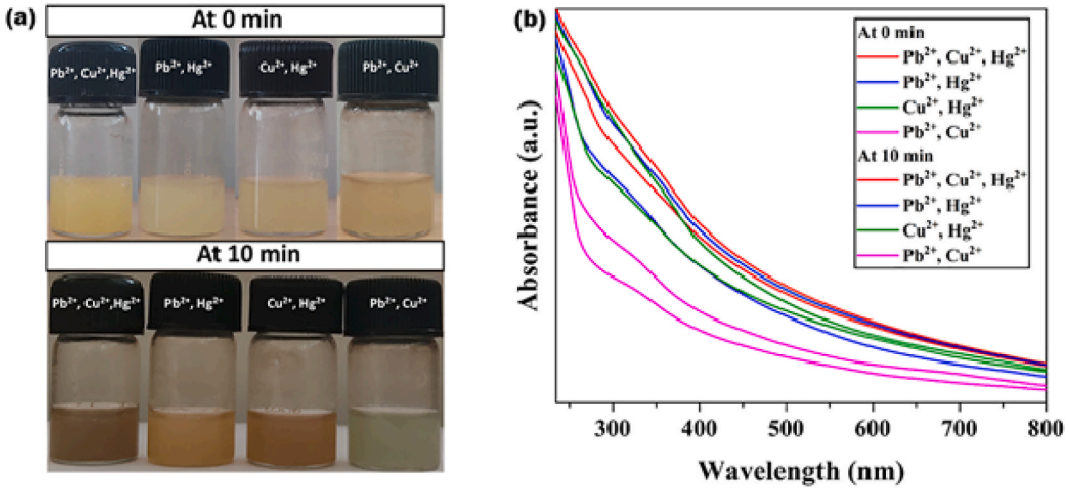

Fig. 12. (a) Colorimetric and (b) UV–Visible spectroscopic measurements of ZnS@β-CD NP added with multiple metal ions (10^{-3} M of Pb^{2+}, Cu^{2+}, &Hg^{2+}, Pb^{2+} & Hg^{2+}, Cu^{2+} & Hg^{2+}, and Pb^{2+} & Cu^{2+}) at 0 min and 10 min.

demonstrates that the absorption peak for ZnS diminished at 10^{-6} M of Hg^{2+}. On the other hand, a further drop in the absorption peak of ZnS was observed for 10^{-5} and 10^{-4} M concentrations of Hg^{2+}, which could be due to the interaction of Hg^{2+} with S^{2-}. Hg^{2+} and Zn^{2+} ions began a partial cation exchange process, which led to the production of $Zn_{1-x}Hg_xS$ NSs, the value of x increases as intensifications of Hg^{2+} ion. At higher Hg^{2+} concentration (10^{-3} –10^{-1} M), the absorbance peak of ZnS NP completely disappeared.

Further, colorimetric, and spectrophotometric time-based interaction studies were performed for ZnS colloidal solution, which was added with 10^{-6} to 10^{-1} M of Hg^{2+}. No substantial change was observed with the addition of a lower concentration of Hg^{2+}. Surprisingly, the addition of 10^{-1} M Hg^{2+} solution showed a color change from bright yellow to white within 10 min of exposure (Fig. 11 (c)). A spectrophotometric response was recorded after 10 min. The UV–Visible spectra in Fig. 11 (d) show the emergence of a new absorption peak at 310 nm, which could be due to the generation of mercury sol (Hg^0) [45,46]. The diminished color in Fig. 9 (a) for the 10^{-1} M concentration of Hg^{2+} is due to the formation of mercury sol. Electrochemical series indicate that the metal ions with relatively high reduction potential have a higher tendency for reduction. The reduction potential of Hg^{2+} is more significant than other metal ions. Even a very mild reducing agent can cause a reduction of Hg^{2+} to Hg^0, and further, it can combine with other metals to generate amalgam. A study has shown that Hg^{2+} in high chloride concentration strongly proclivities to produce mercury sol [47]. The role of capping agents in CER is not widely explored. In CER-based mercury detection, a starch-capped ZnS nanoparticle has shown a similar reduction of higher concentration of Hg^{2+} to mercury sol [21]. Here, the capping agent β-CD contains 7 primary and 14 secondary hydroxyl groups, which may act as a reducing site. The literature report reveals the reducing nature of β-CD for synthesizing inverted core-shell bimetallic NPs and Ag or Au NPs in an aqueous media [48–50]. To confirm the reducing nature of β-CD, an unmodified ZnS NP colloidal solution synthesized without β-CD was added with 10^{-1} M of Hg^{2+} ion and it turned to yellow color. However, this colloidal solution did not turn to white even after 50 min and maintained the initial yellow color throughout. Therefore, when ZnS@β-CD NPs is exposed to a higher concentration of Hg^{2+}, it efficiently reduces to Hg^0, favored by the reducing behavior of β-CD.

3.9. CER sensing of ZnS@β-CD in simultaneous presence of Pb^{2+}, Cu^{2+}, and Hg^{2+} metal ions

Competitive experiments were conducted to assess the CER of Pb^{2+}, Cu^{2+}, and Hg^{2+} metal ions with ZnS@β-CD NPs. A 5 mL of ZnS NP colloidal solution taken in different glass vial was added concurrently with 3 drops of 10^{-3} M concentration of all the three metal ions (Pb^{2+}, Cu^{2+}, and Hg^{2+}) and two metal ions combinations (Pb^{2+} & Hg^{2+}, Cu^{2+} & Hg^{2+}, and Pb^{2+} & Cu^{2+}). Later, their colorimetric and spectrophotometric responses were recorded.

The photographs of ZnS NP colloidal solution with multiple metal ions at 0 min and 10 min are given in Fig. 12 (a). The simultaneous addition of Pb^{2+}, Cu^{2+}, and Hg^{2+} metal ions to ZnS@β-CD NPs turned white-colored colloidal solution to a yellow color, which indicates the preference for Hg^{2+} ion among other ions in CER. After 10 min, the yellow-colored solution turned into a coffee-brown color. The color change from yellow to coffee brown confirms the presence of Pb^{2+} and Cu^{2+} ions and their CER with ZnS NP. Then, among the combination of Pb^{2+} and Hg^{2+} metal ions rendered a color change from white to yellow which once again indicating prompt CER of Hg^{2+} ions with ZnS NPs. After 10 min, the solution changed from yellow to light brown, indicating the presence of Pb^{2+} ions and its CER with ZnS NP. When Cu^{2+} and Hg^{2+} metal ions were added together, a white-colored ZnS NP colloidal solution became yellow, revealing the presence of Hg^{2+} ions in the solution. This demonstrates that Hg^{2+} ions perform an immediate CER with ZnS NPs compared to Cu^{2+} or Pb^{2+} metal ions. After 10 min, the solution's color changed from yellow to medium brown, indicating the existence of Cu^{2+} ion and its CER with ZnS NP. When Pb^{2+} and Cu^{2+} ions were added together, the white color of ZnS NP colloidal solution changed to a light orange color, indicating the preference for Pb^{2+} ion in CER reaction among Pb^{2+} and Cu^{2+} ions. Interestingly, after 10 min, the solution changed to an ash color, which was attributed to the presence of Cu^{2+} ion and its CER with ZnS NP. According to the

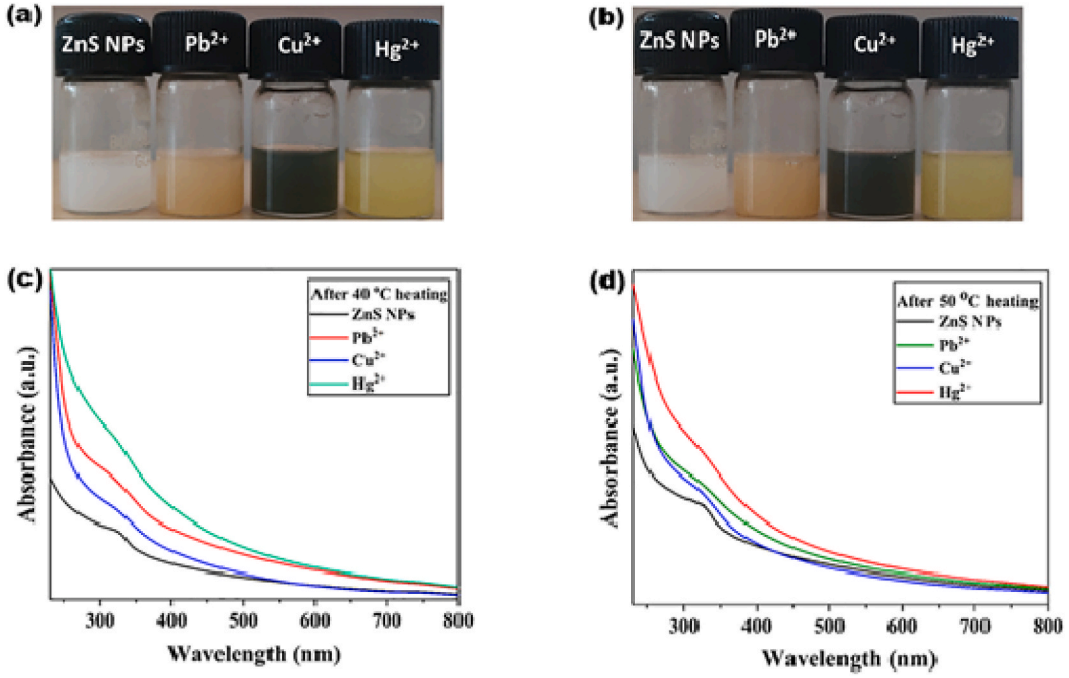

Fig. 13. Colorimetric responses of ZnS@β-CD towards 10^{-3} M concentrations of Pb^{2+}, Cu^{2+}, and Hg^{2+} metal ions (a) at 40 °C and (b) at 50 °C. UV–Visible spectroscopic measurements of ZnS@β-CD NPs towards 10^{-3} M concentrations of Pb^{2+}, Cu^{2+}, and Hg^{2+} metal ions (c) at 40 °C and (d) at 50 °C.

colorimetric responses based on time, the CER of metal ions with ZnS NP may follow the order of Hg^{2+}, Pb^{2+}, and Cu^{2+}, respectively. Fig. 12 (b) depicts the UV–Visible spectra of ZnS NPs added with different combinations of metal ions at 0 min and 10 min. The spectra show that at 0 min, ZnS NPs added with 3 (Pb^{2+}, Cu^{2+}, and Hg^{2+}) and 2 (Pb^{2+} & Hg^{2+}, Cu^{2+} & Hg^{2+}, and Pb^{2+} & Cu^{2+}) metal ions underwent CER and resulted in the complete disappearance of ZnS NP absorption peak at 323 nm. The spectra recorded after 10 min for all metal ion combinations show a rise in the absorbance after their color change. This increase in absorbance indicates the CER of multiple metal ions present in the solution with ZnS NPs.

3.10. Effect of temperature and pH

The effect of temperature on the stability and CER metal sensing abilities of ZnS@β-CD NPs was assessed. For this, a colloidal solution of ZnS NPs was heated for 15 min at 40 and 50 °C then allowed to cool to room temperature. A 5 mL of this colloidal solution taken in glass vials were added with 0.5 mL of 10^{-3} M concentrations of Pb^{2+}, Cu^{2+}, and Hg^{2+} metal ions and their colorimetric and photometric responses were recorded after 5 min of reaction. The photographs given in Fig. 13 (a) and (b) indicate that white-colored ZnS colloidal solutions heated at 40 and 50 °C were changed to orange, black, and bright yellow after adding metal ions Pb^{2+}, Cu^{2+}, and Hg^{2+}, respectively. The corresponding UV–Visible absorption responses are shown in Fig. 13 (c) and (d). These results demonstrate that ZnS@β-CD NPs are quite stable even at 50 °C.

Further, the stability and CER metal detecting capabilities of ZnS@β-CD NPs were evaluated with respect to different pH. ZnS NPs were dispersed in an aqueous medium of different pH (4, 5, 6, 8, 9, and 10). 5 mL of ZnS NP colloidal solution in each pH medium were added with 0.5 mL of 10^{-3} M concentrations of Pb^{2+}, Cu^{2+}, and Hg^{2+} metal ions. After 5 min, their colorimetric CER metal sensing responses were recorded as shown in Fig. 14a. Further, their spectrophotometric responses were carried out and presented in Fig. 14 (b–g). These results also confirm that ZnS@β-CD NPs in different pH solutions have identical colorimetric and photometric CER responses. Hence, the CER based metal sensing of ZnS@β-CD NP is pH stable.

3.11. Limit of detection of ZnS@β-CD NPs

The colorimetric and spectrophotometric limit of detection (LOD) on the CER sensing of ZnS@β-CD NPs towards Pb^{2+}, Cu^{2+}, and Hg^{2+} ions were found to be 1, 10, and 1 μM, respectively. Table 2 compares the colorimetric performance of the proposed sensor to that of existing colorimetric sensors described in the literature [51–57]. Our proposed ZnS@β-CD NPs CER based sensor LOD is as similar as starch-capped ZnS quantum dots.

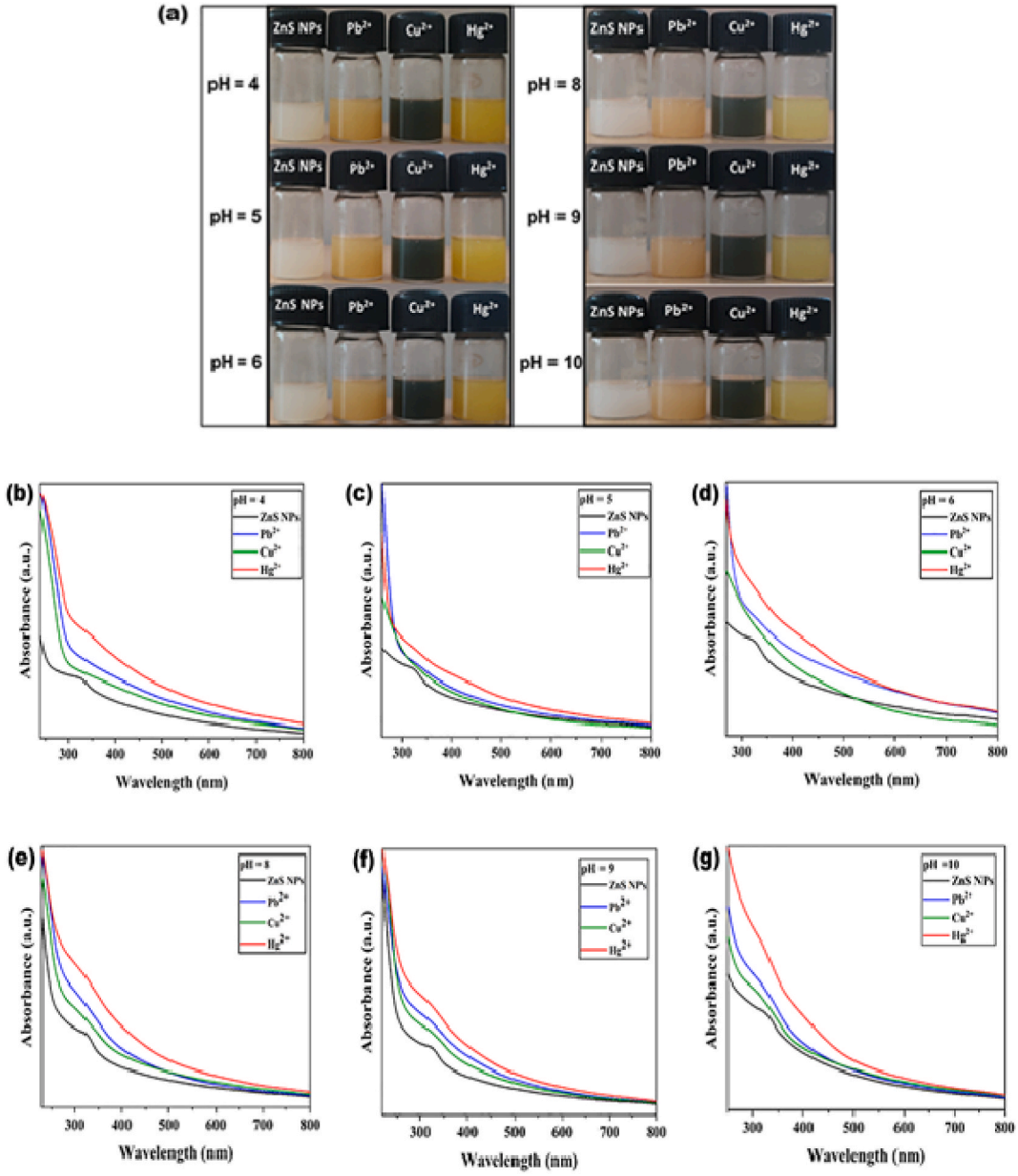

Fig. 14. (a) Colorimetric and (b–g) UV–Visible spectroscopic measurements of ZnS@β-CD NP in different pH medium in presence of 10^{-3} M concentrations of Pb^{2+}, Cu^{2+} and Hg^{2+}.

3.12. FT-IR analysis of ZnS@β-CD NPs and converted products

FT-IR spectroscopic studies were carried out for the structural analysis of ZnS@β-CD NPs, and CER converted NSs (PbS, CuS, and HgS). FT-IR spectrum in Fig. 15 confirms remarkable structural differences after the CER reaction of ZnS@β-CD NPs with the respective metal ions. The ZnS spectra include IR bands at 644 cm^{-1}, 998 cm^{-1}, and 1114 cm^{-1}, which support the formation of ZnS NPs [58]. The other two peaks, 3383 cm^{-1} and 1627 cm^{-1}, represent the O–H stretching and bending frequencies, respectively [58]. The formation of PbS NS was confirmed by the presence of vibrational peaks at 597, 1058, and 1368 cm^{-1}, which are attributed to Pb–S vibration [59]. Likewise, peaks at 589 cm^{-1} and 1084 cm^{-1} are confirming the CuS NS formation [60]. In addition, the vibrational peak at 464 cm^{-1} supported the formation of HgS NSs [61]. For the FT-IR study, 10^{-2} M concentration of Hg^{2+} solution was used to interact with ZnS nanoparticle instead of 10^{-1} M solution. Therefore, the FT-IR spectra could disclose the formation and CER-assisted conversion of ZnS@β-CD NPs to PbS, CuS, and HgS NSs.

Table 2
Comparison of LOD of ZnS@β-CD NPs with published colorimetric sensors for detecting Pb^{2+}, Cu^{2+}, and Hg^{2+} metal ions.

Quantitaive method	Metal ion	Sensor	LOD	References
Colorimetry	Pb^{2+}	AuNP	1.8 μM	51
		AuNP	2.5 μM	52
		AgNP	1 μM	53
		ZnS NP	1 μM	21
		ZNS NP	1 μM	Proposed method
		ZnS NP	1.24 μM	54
	Cu^{2+}	AuNP	0.5 μM	55
		AgNP	2.9 μM	56
		ZnS NP	10 μM	21
		ZnS NP	10 μM	Proposed method
	Hg^{2+}	AuNP	3 μM	52
		AgNP	11.17 μM	53
		CdSe/ZnS QD	0.09 μM	57
		ZnS NP	1 μM	21
		ZnS NP	1 μM	Proposed method

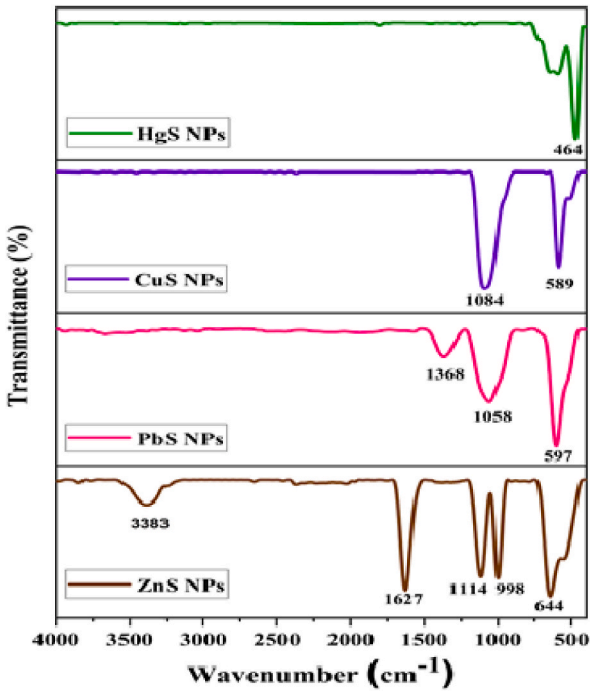

Fig. 15. FT-IR spectra of ZnS@β-CD NPs and its CER converted products.

4. Conclusion

In summary, we have reported a simple method for synthesizing ZnS@β-CD NPs and several spectroscopic techniques were used to characterize these NPs. Synthesized ZnS@β-CD NPs were utilized for CER-assisted colorimetric detection of Pb^{2+}, Cu^{2+}, and Hg^{2+} in the aqueous media. The Pb^{2+}, Cu^{2+}, and Hg^{2+} ions changed to orange, black, and bright yellow colors. The colorimetric changes were confirmed using UV–Visible spectrophotometric analysis. A partial CER led to the formation of Zn_{1-x}, Pb_xS, $Zn_{1-x}Cu_xS$ and $Zn_{1-x}Hg_xS$ for the corresponding metal ion, whereas a complete CER led to the formation of PbS, CuS and HgS. The partial and complete CER could be categorized based on the color difference of transformed products. Also, the ZnS@β-CD NPs are capable of distinguishing and determining various Pb^{2+}, Cu^{2+}, and Hg^{2+} concentrations. The proposed method holds multiple benefits, such as simple, low-cost, solvent-free, facile, and naked-eye detection of metal ions.

Data availability

Data will be made available on request.

CRediT authorship contribution statement

Vyshnavi T. Veetil: Data curation, Formal analysis, Investigation, Methodology, Writing – original draft. **Anakha D. Rajeeve:** Data curation, Formal analysis, Validation. **Saran G.P:** Methodology. **K.S. Manish Kumar:** Methodology. **M. Bhagiyalakshmi:** Software, Validation. **Mari Vinoba:** Software, Validation. **R. Yamuna:** Conceptualization, Investigation, Supervision, Validation, Writing – review & editing.

Declaration of competing interest

The authors declare that they have no known competing financial interests or personal relationships that could have appeared to influence the work reported in this paper.

Acknowledgements

We are grateful to CoE-AMGT center (MHRD, New Delhi) for providing instrumental facilities. We also thank ACNSMM, AIMS Kochi for recording XPS and TEM images.

References

[1] A.V. Kalarikkandy, N. Sree, S. Ravichandran, G. Dheenadayalan, Copolymer - MnO_2 nanocomposites for the adsorptive removal of organic pollutants from water, Environ. Sci. Pollut. Control Ser. 30 (2023) 71454–71463, https://doi.org/10.1007/s11356-022-22137-2.
[2] K. A.V.K, D. Gangadharan, Nano-Structures & Nano-Objects Adsorptive remediation of organic pollutant and arsenic (V) ions from water using Fe_3O_4 -MnO_2 nanocomposite, Nano-Structures & Nano-Objects 29 (2022), 100837, https://doi.org/10.1016/j.nanoso.2022.100837.
[3] M. Jaishankar, T. Tseten, N. Anbalagan, B.B. Mathew, K.N. Beeregowda, Toxicity, mechanism and health effects of some heavy metals, Interdiscipl. Toxicol. 7 (2014) 60–72, https://doi.org/10.2478/intox-2014-0009.
[4] P.B. Tchounwou, C.G. Yedjou, A.K. Patlolla, D.J. Sutton, Heavy metal toxicity and the environment, Molecular, Clinical and Environ. Toxicicol. 3 (2012) 133–164, https://doi.org/10.1007/978-3-7643-8340-4.
[5] K. Aoki, M. Aschner, J.T. Cullen, E. Farkas, M. Filella, P. Hauser, K. Klotz, H. Küpper, W. Maret, T.J. Stewart, M.J. Stillman, V.L. Pecoraro, H.R. Pohl, B. Tylkowski, Lead: its Effects on Environment and Health, Walter de Gruyter GmbH & Co KG, 2017, p. 17, https://doi.org/10.1515/9783110434330.
[6] M.E. Street, K. Audouze, J. Legler, H. Sone, P. Palanza, Endocrine disrupting chemicals: current understanding, new testing strategies and future research needs, Int. J. Mol. Sci. 22 (2021) 1–5, https://doi.org/10.3390/ijms22020933.
[7] B. Weiss, Lead, manganese, and methylmercury as risk factors for neurobehavioral impairment in advanced age, Int. J. Alzheimer's Dis. 2011 (2011), https://doi.org/10.4061/2011/607543.
[8] T. Sanders, Y. Liu, V. Buchner, P.B. Tchounwou, Neurotoxic effects and biomarkers of lead exposure: a review, Rev. Environ. Health 24 (2009) 15–45, https://doi.org/10.1515/REVEH.2009.24.1.15.
[9] G.T. Strickland, W.M. Beckner, M.L. Leu, Absorption of copper in homozygotes and heterozygotes for Wilson's disease and controls: isotope tracer studies with ^{67}Cu and ^{64}Cu, Clin. Sci. 43 (1972) 617–625, https://doi.org/10.1042/cs0430617.
[10] M. Harada, Minamata disease: methylmercury poisoning in Japan caused by environmental pollution, Crit. Rev. Toxicol. 25 (1995) 1–24, https://doi.org/10.3109/10408449509089885.
[11] S. Han, X. Qin, Z. An, Y. Zhu, L. Liang, Y. Han, W. Huang, X. Liu, Multicolour synthesis in lanthanide-doped nanocrystals through cation exchange in water, Nat. Commun. 7 (2016) 1–7, https://doi.org/10.1038/ncomms13059.
[12] Z. Zhang, S. Dai, X. Fan, D.A. Blom, S.J. Pennycook, Y. Wei, Controlled synthesis of CdS nanoparticles inside ordered mesoporous silica using ion-exchange reaction, J. Phys. Chem. B 105 (2001) 3–6, https://doi.org/10.1021/jp010541q.
[13] V. Lesnyak, C. George, A. Genovese, M. Prato, A. Casu, S. Ayyappan, A. Scarpellini, L. Manna, Alloyed copper chalcogenide nanoplatelets via partial cation exchange reactions, ACS Nano 8 (2014) 8407–8418, https://doi.org/10.1021/nn502906z.
[14] D.H. Son, S.M. Hughes, Y. Yin, A.P. Alivisatos, Cation exchange reactions in ionic nanocrystals, ChemInform 36 (2005) 1009–1013, https://doi.org/10.1002/chin.200508244.
[15] Y. Hong, S. Venkateshalu, S. Jeong, J. Park, K. Lee, Regiospecific cation exchange in nanocrystals and its potential in diversifying the nanostructural library, Small Sci 3 (2023), 2200063, https://doi.org/10.1002/smsc.202200063.
[16] M. Jiao, Y. Li, Y. Jia, Z. Yang, X. Luo, Aqueously synthesized color-tunable quaternary Cu-In-Zn-S quantum dots for Cu(II) detection via mild and rapid cation exchange, Sens. Actuators, B 294 (2019) 32–39, https://doi.org/10.1016/j.snb.2019.05.027.
[17] K. Huang, K. Xu, J. Tang, L. Yang, J. Zhou, X. Hou, C. Zheng, Room temperature cation exchange reaction in nanocrystals for ultrasensitive speciation analysis of silver ions and silver nanoparticles, Anal. Chem. 87 (2015) 6584–6591, https://doi.org/10.1021/acs.analchem.5b00511.
[18] L.Q. Lu, T. Tan, X.K. Tian, Y. Li, P. Deng, Visual and sensitive fluorescent sensing for ultratrace mercury ions by perovskite quantum dots, Anal. Chim. Acta 986 (2017) 109–114, https://doi.org/10.1016/j.aca.2017.07.014.
[19] A. Sadollahkhani, A. Hatamie, O. Nur, M. Willander, B. Zargar, I. Kazeminezhad, Colorimetric disposable paper coated with ZnO@ZnS Core−Shell nanoparticles for detection of copper ions in aqueous solutions, ACS Appl. Mater. Interfaces 6 (2014) 17694–17701, https://doi.org/10.1021/am505480y.
[20] A. Jaiswal, S.S. Ghsoh, A. Chattopadhyay, Quantum dot impregnated-chitosan film for heavy metal ion sensing and removal, Langmuir 28 (2012) 15687–15696, https://doi.org/10.1021/la3027573.
[21] S. Bano, S.I. Raj, A. Khalilullah, A. Jaiswal, I. Uddin, Selective and sensitive cation exchange reactions in the aqueous starch capped ZnS nanoparticles with tunable composition, band gap and color for the detection and estimation of Pb^{2+}, Cu^{2+} and Hg^{2+}, J. Photochem. Photobiol. Chem. 405 (2021), 112925 https://doi.org/10.1016/j.jphotochem.2020.112925.
[22] T.T. Quynh Hoa, L. Van Vu, T.D. Canh, N.N. Long, Preparation of ZnS nanoparticles by hydrothermal method, J. Phys. Conf. Ser. 187 (2009), https://doi.org/10.1088/1742-6596/187/1/012081.
[23] J. Aswathy, N.V. Seethalekshmy, K.R. Hiran, M.R. Bindhu, K. Manzoor, S.V. Nair, D. Menon, Mn-doped zinc sulphide nanocrystals for immunofluorescent labeling of epidermal growth factor receptors on cells and clinical tumor tissues, Nanotechnology 25 (2014), https://doi.org/10.1088/0957-4484/25/44/445102.
[24] K. Saito, K. McGehee, Y. Norikane, Size-controlled synthesis of cyclodextrin-capped gold nanoparticles for molecular recognition using surface-enhanced Raman scattering, Nanoscale Adv. 3 (2021) 3272–3278, https://doi.org/10.1039/d1na00125f.
[25] D.D. Gadade, S.S. Pekamwar, Cyclodextrin based nanoparticles for drug delivery and theranostics, Adv. Pharmaceut. Bull. 10 (2020) 166–183, https://doi.org/10.34172/apb.2020.022.
[26] D. Pandey, V.S. Panwar, H. Mishra, L. Adhikari, M. Pandey, M. Semalty, Cyclodextrin based nanoparticles for improved solubility and drug delivery, J. Mt. Res. 16 (2021) 187–199, https://doi.org/10.51220/jmr.v16i1.19.

[27] B. Aswathy, G.S. Avadhani, S. Suji, G. Sony, Synthesis of β -cyclodextrin functionalized gold nanoparticles for the selective detection of Pb^{2+} ions from aqueous solution 6 (2012) 168–175, https://doi.org/10.1007/s11706-012-0165-5.

[28] M.R. Bindhu, P. Saranya, M. Sheeba, C. Vijilvani, T.S. Rejiniemon, A.M. Al-mohaimeed, M. Ragab, M. Soliman, Functionalization of gold nanoparticles by β -cyclodextrin as a probe for the detection of heavy metals in water and photocatalytic degradation of textile dye, Environ. Res. 201 (2021), 111628, https://doi.org/10.1016/j.envres.2021.111628.

[29] B. Amanulla, H. Kalyani, R. Subbu, S.K. Ramaraj, A sonochemical synthesis of cyclodextrin functionalized Au-FeNPs for colorimetric detection of Cr^{6+} in different industrial waste water, Ultrason. Sonochem. 42 (2018) 747–753, https://doi.org/10.1016/j.ultsonch.2017.12.041.

[30] Y. Chen, Q.S. Wu, Y.P. Ding, Synthesis and characterization of ZnS nanotubes with crossed-channels, J. Braz. Chem. Soc. 18 (2007) 924–927, https://doi.org/10.1590/S0103-50532007000500008.

[31] P. Scherrer, Bestimmung der Grösse und der inneren Struktur von Kolloidteilchen mittels Röntgenstrahlen, 1918, Nachr. Ges. Wiss. Göttingen. Mathematisch-Physikalische Klasse (1918) 98–100, http://eudml.org/doc/59018.

[32] N. Mintcheva, G. Gicheva, M. Panayotova, S.A. Kulinich, Room-temperature synthesis of zns nanoparticles using zinc xanthates as molecular precursors, Materials 13 (2020) 1–12, https://doi.org/10.3390/ma13010171.

[33] Z.H. Ibupoto, K. Khun, X. Liu, M. Willander, Hydrothermal synthesis of nanoclusters of zns comprised on nanowires, Nanomaterials 3 (2013) 564–571, https://doi.org/10.3390/nano3030564.

[34] M. Mao, L. Jiang, L. Wu, M. Zhang, T. Wang, The structure control of ZnS/graphene composites and their excellent properties for lithium-ion batteries, J. Mater. Chem. A 3 (2015) 13384–13389, https://doi.org/10.1039/c5ta01501d.

[35] A. Pendashteh, M.F. Mousavi, M.S. Rahmanifar, Fabrication of anchored copper oxide nanoparticles on graphene oxide nanosheets via an electrostatic coprecipitation and its application as supercapacitor, Electrochim. Acta 88 (2013) 347–357, https://doi.org/10.1016/j.electacta.2012.10.088.

[36] D.S. Abraham, M. Chandran, M. Vinoba, R. Yamuna, M. Bhagiyalakshmi, Flower-like layered NiCu-LDH/MXene nanocomposites as an anodic material for electrocatalytic oxidation of methanol, Langmuir (2023), https://doi.org/10.1021/acs.langmuir.3c00154.

[37] L. Liu, X. Chen, Z. Wang, X. Wang, S. Lin, The removal mechanism and performance of tetrabromobisphenol A with a novel multi-group activated carbon from recycling long-root: Eichhornia crassipes plants, RSC Adv. 9 (2019) 24760–24769, https://doi.org/10.1039/c9ra03374b.

[38] M. Schindler, F.C. Hawthorne, M.S. Freund, P.C. Burns, XPS spectra of uranyl minerals and synthetic uranyl compounds. II: the O 1s spectrum, Geochem. Cosmochim. Acta 73 (2009) 2488–2509, https://doi.org/10.1016/j.gca.2008.10.041.

[39] D. Prema, S. Thamaraiselvi, R. Yamuna, Encapsulation of N-phenyl p-phenylenediamine into β-CD: spectral, molecular modelling studies and sensor application for detecting Fe^{2+} ion, J. Mol. Liq. 319 (2020), 113990, https://doi.org/10.1016/j.molliq.2020.113990.

[40] C.N.R. Rao, A. Mu, A.K. Cheetham, The chemistry of nanomaterials, Chem. Nanomater. (2004), https://doi.org/10.1002/352760247x.

[41] K.R. Bindu, T.A. Safeera, E.I. Anila, Pure red luminescence and concentration-dependent tunable emission color from europium-doped zinc sulfide nanoparticles, J. Mater. Sci. Mater. Electron. 33 (2022) 17793–17801, https://doi.org/10.1007/s10854-022-08644-5.

[42] M. Jothibas, C. Manoharan, S. Johnson Jeyakumar, P. Praveen, I. Kartharinal Punithavathy, J. Prince Richard, Synthesis and enhanced photocatalytic property of Ni doped ZnS nanoparticles, Sol. Energy 159 (2018) 434–443, https://doi.org/10.1016/j.solener.2017.10.055.

[43] J. Tauc, R. Grigorovici, A. Vancu, Optical properties and electronic structure of amorphous germanium, Phys. Status Solidi 15 (1966) 627–637, https://doi.org/10.1002/pssb.19660150224.

[44] R. Viswanath, H.S.B. Naik, Y.K.G. Somalanaik, P.K.P. Neelanjeneallu, K.N. Harish, M.C. Prabhakara, Studies on characterization, optical absorption, and photoluminescence of yttrium doped ZnS nanoparticles, J. Nanotechnol. 2014 (2014), https://doi.org/10.1155/2014/924797.

[45] A. Henglein, C. Brancewicz, Absorption spectra and reactions of colloidal bimetallic nanoparticles containing mercury, Chem. Mater. 9 (1997) 2164–2167, https://doi.org/10.1021/cm970258x.

[46] L. Katsikas, M. Gutiérrez, A. Henglein, Bimetallic colloids: silver and mercury, J. Phys. Chem. 100 (1996) 11203–11206, https://doi.org/10.1021/jp960357i.

[47] Q. Wang, W. Qin, L. Chai, Q. Li, Understanding the formation of colloidal mercury in acidic wastewater with high concentration of chloride ions by electrocapillary curves, Environ. Sci. Pollut. Res. 21 (2014) 3866–3872, https://doi.org/10.1007/s11356-013-2379-1.

[48] V.I. Bhoi, S. Kumar, C.N. Murthy, Cyclodextrin encapsulated monometallic and inverted core-shell bimetallic nanoparticles as efficient free radical scavengers, New J. Chem. 40 (2016) 1396–1402, https://doi.org/10.1039/c5nj02511g.

[49] K. Yang, J. Liu, L. Luo, M. Li, T. Xu, J. Zan, Synthesis of cationic β-cyclodextrin functionalized silver nanoparticles and their drug-loading applications, RSC Adv. 13 (2023) 7250–7256, https://doi.org/10.1039/d2ra08216k.

[50] K. Saito, K. McGehee, Y. Norikane, Size-controlled synthesis of cyclodextrin-capped gold nanoparticles for molecular recognition using surface-enhanced Raman scattering, Nanoscale Adv. 3 (2021) 3272–3278, https://doi.org/10.1039/d1na00125f.

[51] Y. Yu, S.S. Naik, Y. Oh, J. Theerthagiri, S.J. Lee, Lignin-mediated green synthesis of functionalized gold nanoparticles via pulsed laser technique for selective colorimetric detection of lead ions in aqueous media, J. Hazard Mater. 420 (2021), 126585, https://doi.org/10.1016/j.jhazmat.2021.126585.

[52] R. Gunupuru, D. Maity, G. Vyas, P. Paul, Water dispersible glycylglycine functionalized gold nanoparticles : application in colorimetric sensing of Hg (II), Pb (II) and Cr (III) in aqueous media, J. Chem. Sci. (2022), 0123456789, https://doi.org/10.1007/s12039-022-02078-6.

[53] V.V. Kumar, S.P. Anthony, Silver nanoparticles based selective colorimetric sensor for Cd^{2+}, Hg^{2+} and Pb^{2+} ions: tuning sensitivity and selectivity using co-stabilizing agents, Sens. Actuators, B 191 (2014) 31–36, https://doi.org/10.1016/j.snb.2013.09.089.

[54] P. Uddandarao, R.M. Balakrishnan, Thermal and optical characterization of biologically synthesized ZnS nanoparticles synthesized from an endophytic fungus Aspergillus flavus: a colorimetric probe in metal detection, Spectrochim. Acta Part A Mol. Biomol. Spectrosc. 175 (2017) 200–207, https://doi.org/10.1016/j.saa.2016.12.021.

[55] Y. Ye, M. Lv, X. Zhang, Y. Zhang, Colorimetric determination of copper(II) ions using gold nanoparticles as a probe, RSC Adv. 5 (2015) 102311–102317, https://doi.org/10.1039/c5ra20381c.

[56] N. Ratnarathorn, O. Chailapakul, C.S. Henry, W. Dungchai, Simple silver nanoparticle colorimetric sensing for copper by paper-based devices, Talanta 99 (2012) 552–557, https://doi.org/10.1016/j.talanta.2012.06.033.

[57] H. Li, W. Wang, Z. Wang, Q. Lv, H. Bai, Q. Zhang, Analyte-enhanced photocatalytic activity of CdSe/ZnS quantum dots for paper-based colorimetric sensing of Hg^{2+} under visible light, Microchem. J. 164 (2021), https://doi.org/10.1016/j.microc.2021.106037.

[58] P. Iranmanesh, S. Saeednia, M. Nourzpoor, Characterization of ZnS nanoparticles synthesized by co-precipitation method, Chin. Phys. B 24 (2015), https://doi.org/10.1088/1674-1056/24/4/046104.

[59] U. Priyanka, A. Gowda K M, E. M G, S. Teja B, N. Nitish, R. Mohan B, Biologically synthesized PbS nanoparticles for the detection of arsenic in water, Int. Biodeterior. Biodegrad. 119 (2017) 78–86, https://doi.org/10.1016/j.ibiod.2016.10.009.

[60] J. Theerthagiri, R.A. Senthil, A. Malathi, A. Selvi, J. Madhavan, M. Ashokkumar, Synthesis and characterization of a CuS-WO_3 composite photocatalyst for enhanced visible light photocatalytic activity, RSC Adv. 5 (2015) 52718–52725, https://doi.org/10.1039/c5ra06512g.

[61] H. Safardoust-Hojaghan, M. Shakouri-Arani, M. Salavati-Niasari, Structural and spectroscopic characterization of HgS nanoparticles prepared via simple microwave approach in presence of novel sulfuring agent, Trans. Nonferrous Metals Soc. China 26 (2016) 759–766, https://doi.org/10.1016/S1003-6326(16)64166-3.